J. Fluid Mech. (2001), *vol.* 438, *pp.* 101–128. Printed in the United Kingdom

Fluidization by lift of 300 circular particles in plane Poiseuille flow by direct numerical simulation

By HYOUNG G. CHOI† AND DANIEL D. JOSEPH

Department of Aerospace Engineering and Mechanics, 107 Akerman Hall, 110 Union Street SE, University of Minnesota, Minneapolis, MN 55455, USA

(Received 11 March 2000 and in revised form 5 October 2000)

We study the transport of a slurry of heavier-than-liquid circular particles in a plane pressure-driven flow in a direct simulation. The flow is calculated in a periodic domain containing 300 circular particles. The study leads to the concept of fluidization by lift in which all the particles are suspended by lift forces against gravity perpendicular to the flow. The study is framed as an initial-value problem in which a closely packed cubic array of particles resting on the bottom of the channel is lifted into suspension. All the details of the flow are resolved numerically without model assumptions. The fluidization of circular particles first involves bed inflation in which liquid is driven into the bed by high pressure at the front and low pressure at the back of each circle in the top row. This kind of bed inflation occurs even at very low Reynolds numbers but it takes more time for the bed to inflate as the Reynolds number is reduced. It appears that the bed will not inflate if the shear Reynolds number is below the critical value for single particle lift-off. The flows with a single particle are completely determined by a shear Reynolds number and a gravity parameter when the density ratio and aspect ratio parameters are specified. In the multi-particle case, the volume fraction and distribution also matters. The transition to a fully fluidized slurry by waves is discussed.

An analytical model of the steady motion of a single particle dragged forward in a Poiseuille flow is derived and compared with a simulation. The undisturbed fluid velocity is always larger than the particle velocity, producing a fluid hold-up. The effect of the hold-up in the many particle case is to greatly reduce the velocity of the mixture which may be described by a two-fluid model in which the solid laden mixture is regarded as a second fluid with effective properties.

1. Introduction

The problem of transport of particles by fluids in horizontal conduits and pipes is of considerable scientific and industrial importance and is the focus of this paper. This problem arises in the transport of coal–water slurries, in the removal of drill cuttings in the drilling of horizontal oil wells and in proppant transport in hydraulically fractured rock in oil- and gas-bearing reservoirs, to name a few examples. The central unsolved fluid dynamics problem arising in these applications is fluidization by lift.

† Present address: BK21, Mechanical Engineering Research Division, Seoul National University, Seoul 151–742, Korea.

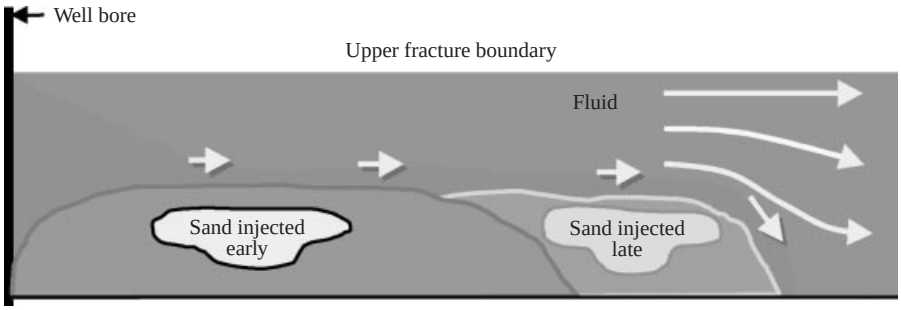

FIGURE 1. Sand transport in a fractured reservoir (after Kern, Perkins & Wyant 1959).

The problem of fluidization by lift can be framed well in the problem of hydraulic fracturing.

Hydraulic fracturing is a process often used to increase the productivity of a hydrocarbon well. A slurry of sand in a highly viscous, sometimes elastic, fluid is pumped into the well to be stimulated at sufficient pressure to exceed the horizontal stresses in the rock at reservoir depth. This opens a vertical fracture, some hundreds of feet long, tens of feet high, and perhaps an inch in width, penetrating from the well bore far into the pay zone. When the pumping pressure is removed, the sand acts to prop the fracture open. Productivity is enhanced because the sand-filled fracture offers a higher-conductivity path for fluids to enter the well than through the bulk reservoir rock, and because the area of contact for flow out from the productive formation is increased. It follows that a successful stimulation job requires that there be a continuous sand-filled path from great distances in the reservoir to the well, and that the sand is placed within productive, rather than non-productive, formations.

In a slot problem, a particle laden (say 20% solids) fluid is driven by a pressure gradient and the particles settle to the bottom as they are dragged forward. Sand is deposited on the bottom of the slot; a mound of sand develops and grows until the gap between the top of the slot and the mound of sand reaches an equilibrium value; this value is associated with a critical velocity. The velocity in the gap between the mound and the top of the slot increases as the gap above the mound decreases. For velocities below critical, the mound becomes higher and spreads laterally; for larger velocities, sand will be washed out until the equilibrium height and velocity are reestablished (see figure 1). The physical processes mentioned here are *settling* and *washout*. Washout could be by sliding and slipping; however, a more efficient transport mechanism is by advection after suspension which we studied by direct simulation.

In fluidized beds and sedimentation columns in which particles are in a balance of buoyant weight and drag, the cooperative effects of other nearby particles enter strongly into the dynamics. These effects are described by theories of hindered motion. There is a definite relationship between the fluidization by drag of an isolated particle and the fluidization of a particle in a swarm of other particles; for example, the Richardson–Zaki correlation (Richardson & Zaki 1954). Analogous ideas must come into play in problems of slurries which are fluidized by lift rather than by drag; hindered motion effects involving the effective viscosity and the effective density of a suspension and other cooperative effects surely enter here, but are not well understood.

The problem of lift on a single particle has been treated by many authors in the

low-Reynolds-number limit. Even in the much better understood subject of drag on a single particle, say a drag on a sphere, there are no first principle formulae, and empirical relations must be used. The problem of lift of a single circular particle in Poiseuille flow at finite Reynolds numbers has been studied in direct numerical simulation by Patankar *et al.* (2001); this paper has a discussion of previous work which will not be repeated here.

Patankar *et al.* is based on an ALE method using body-fitted unstructured finite-element grids very closely related to the numerical method introduced by Choi (2000) and used here. A Chorin (1968) type fractional step scheme for particulate flows is introduced in the approach by Choi (2000).

Using the ALE particle mover, Patankar *et al.* studied *lift-off* and *slip-velocity* fluidization in Newtonian and viscoelastic fluids. A heavier than liquid particle is resting on the bottom of a channel in the presence of a shear (Poiseuille) flow. At a certain critical speed, depending on the weight and diameter of the particle, the fluid properties, and the aspect ratio of the channel, the particle rises from the wall to an equilibrium height at which the buoyant weight just balances the upward thrust of fluid forces. The values of the particle velocity, the angular velocity of the particle, the slip velocity and the angular slip velocity at equilibrium together with the values of the relevant dimensionless parameters were tabulated.

We did dynamic simulations of single-particle lift to equilibrium at larger Reynolds numbers and found that the rise and other equilibrium properties are not smooth functions of the pressure gradient but instead exhibit instability and hysteresis. These results can be found in Patankar *et al.* (2001) who showed that the hysteresis loops arise as double turning point solutions. The existence of multiple steady solutions for single particle lifting may have important implications for slurries. Certainly, such considerations are not found in models of solid–liquid flow and it is necessary to visit this question in the future.

In § 4, we carry out studies of fluidization by lift of 300 particles in the same plane Poiseuille flow used to study the lift to equilibrium of a single particle. The computation is carried out in a long periodic domain in which the volume fraction of solid circles ranges roughly between 78% and 31%. The study is framed as an initial-value problem in which a closely spaced cubic array of particles resting on the bottom of the channel is lifted into suspension.

The following picture emerges from this study. At early times, the top of the array is only slightly disturbed; since the cubic crystal array is not tightly packed, the top layers move forward relative to the bottom. The lifting of particles out of suspension is accomplished by a pressure mechanism clearly revealed by the simulation; liquid is driven into the bed by high pressure at the front and low pressure at the back of each circle in the top row. The particles are dislodged by this pressure mechanism. At higher Reynolds numbers, single particles are thrown out of the bed in a manner resembling saltation. Typically, isolated particles will fall back into the bed because the drag on an isolated particle is less than when it is among many. The permanent lifting of more particles of the bed takes shape in the formation of waves, which resemble water waves. The wave amplitude grows as the pressure gradient and flow speed increase; particles are levitated out of the bed and the levitated particles form a fluidized suspension over a fixed bed. This can be described as bed erosion. It is possible to erode the whole bed and fluidize all of the particles by lift if the pressure gradient is high enough and the bed depth small enough. The wave amplitude decreases when the particles are fully fluidized.

The evolution to full fluidization is associated with a transition from a vertical

stratification of dynamic pressure to a horizontal stratification of dynamic pressure. The final state of full fluidization is not steady. Internal pressure waves which propagate horizontally are associated with the propagation of particle-depleted regions which could be described as an internal wave of the volume fraction.

A single heavier-than-liquid particle will not lift off at low pressure gradients; the particle slides and rolls on the wall; lift-off to equilibrium occurs at critical values. In the fluidized suspension, we can track the evolution of the rise of the mass centre of the particles. The final state of full fluidization can be determined as the levelling off of the rise of the mass centre curve. The mass centre did not rise, even after a long computation, when the pressure gradient was below the one critical for the rise of a single particle.

2. Equations of motion and scaling parameters

We use the same scales and equations as Patankar *et al.* (2001), (length, time, velocity, stress) $= (d, \dot{\gamma}_w^{-1}, \dot{\gamma}_w d, \eta\dot{\gamma}_w)$ and find that the governing dimensionless equations for slurry flow of 300 circular particles can be written as

$$R\left[\frac{\partial \boldsymbol{u}}{\partial t} + \boldsymbol{u}\cdot\nabla\boldsymbol{u}\right] = -\nabla p + \frac{2d}{W}\boldsymbol{e}_x + \nabla^2\boldsymbol{u} \quad \text{fluid,} \tag{2.1}$$

$$\left.\begin{aligned} \frac{\rho_p}{\rho_f}R\frac{\mathrm{d}\boldsymbol{U}}{\mathrm{d}t} &= -G\boldsymbol{e}_y + \frac{2d}{W}\boldsymbol{e}_x + \frac{2}{\pi}\int_0^{2\pi}\boldsymbol{\sigma}\,\mathrm{d}\theta \\ \frac{\rho_p}{\rho_f}R\frac{\mathrm{d}\boldsymbol{\Omega}}{\mathrm{d}t} &= \frac{16d}{\pi}\int_0^{2\pi}\boldsymbol{e}_r\wedge\boldsymbol{\sigma}\,\mathrm{d}\boldsymbol{\theta} \end{aligned}\right\} \quad \text{solid,} \tag{2.2}$$

where $\boldsymbol{e}_r$ is the radial unit vector from the centre of the circle; $\boldsymbol{\sigma} = -p\boldsymbol{e}_r + 2\boldsymbol{D}[y]\cdot\boldsymbol{e}_r$ is the stress vector,

$$\left.\begin{aligned} R &= \rho_f\dot{\gamma}_w d^2/\eta \quad \text{shear Reynolds number,} \\ G &= \frac{\rho_p-\rho_f}{\eta\dot{\gamma}_w}gd \quad \text{gravity parameter.} \end{aligned}\right\} \tag{2.3}$$

Instead of R and G we may use the product

$$R_G = RG = \frac{\rho_f(\rho_p-\rho_f)gd^3}{\eta^2}, \tag{2.4}$$

and ratio

$$\frac{R}{G} = \frac{d\dot{\gamma}_w^2}{(\rho_p/\rho_f-1)g}. \tag{2.5}$$

The sedimentation Reynolds number R_G does not depend on $\dot{\gamma}_w$, and the generalized Froude number R/G does not depend on the viscosity η.

Adherence boundary conditions are prescribed also at the boundary of each circle

$$\boldsymbol{u} = \boldsymbol{U} + \boldsymbol{\Omega}\wedge\boldsymbol{e}_r d. \tag{2.6}$$

When, as in a slurry, there are many particles, the number N and places of N boundaries enter into the problem description. In the present case, 300 is the number and the places of these 300 particles evolve as part of the solution. We have similarity then for all evolution problems for which N, d/W, ρ_p/ρ_f, R and G are identical. In fact, the density ratio ρ_p/ρ_f enters only in (2.2) as the coefficient of the acceleration

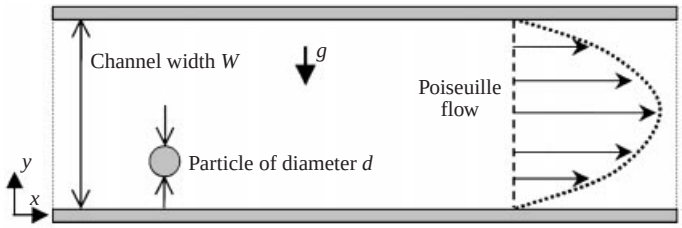

FIGURE 2. Levitation of a heavier-than-liquid particle in a plane Poiseuille flow. The disturbed flow is periodic with period L.

terms, hence, does not enter for steady flow. Though steady flows of a single particle do occur and were studied by Patankar *et al.* (2001), steady flow of many particles do not appear to occur in the multiple particle case after lift off; however, it is possible that the accelerations are small after the bed has fully expanded.

3. Problem formulation

The problem to be considered is the levitation of particles of diameter d in a plane Poiseuille flow in a horizontal channel of width W as shown in figure 2.

The undisturbed Poiseuille flow is given by

$$\left.\begin{aligned} U(y) &= 4U_m \frac{y}{W}\left(1-\frac{y}{W}\right), \\ U_m &= U\left(\frac{W}{2}\right) = \frac{W^2\bar{p}}{8\eta}, \\ \dot{\gamma} &= \frac{\mathrm{d}u}{\mathrm{d}y}, \\ \dot{\gamma}_w &= \frac{4U_m}{W} = \frac{W\bar{p}}{2\eta}. \end{aligned}\right\} \tag{3.1}$$

The presence of particles disturbs the Poiseuille flow. It is assumed that the disturbance flow, satisfying equations (2.1) and (2.2) is periodic with period L. This periodicity is strictly enforced in the computation by the construction of a periodic mesh. The solution of the disturbance flow depends on L, but only weakly for large L. We used

$$L = 22d \quad \text{for single particle,} \quad L = 63d \quad \text{for 300 particles.}$$

All the calculations were carried out in dimensional variables using CGS units. The height of the channel is $W = 12d$ and $d = 1$ cm. The particle density is $\rho_p = 1.01\rho_f$ and the fluid density $\rho_f = 1\,\mathrm{g\,cm^{-3}}$. Calculations were made for three different viscosities $\eta = 1$, 0.2 and 0.01 poise, from light oil to water. For each η, the calculations were carried out for different pressure gradient $\bar{p}$ in $\mathrm{dyn\,cm^{-3}}$.

The results of calculations in dimensional variables may be generalized by post processing. In the present case, ρ_p/ρ_f, d/W, d/L and the number of particles in a cell are fixed, and flows are completely determined by the shear Reynolds number R and gravity number G given by (2.3).

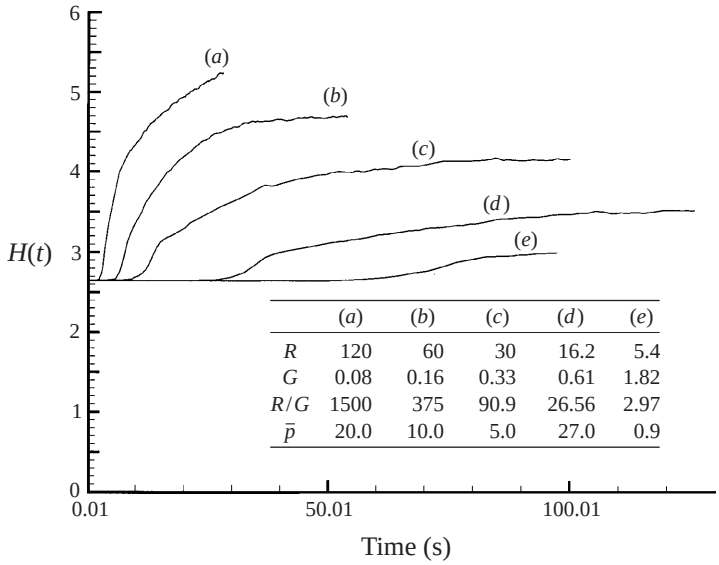

	(a)	(b)	(c)	(d)	(e)
R	120	60	30	16.2	5.4
G	0.08	0.16	0.33	0.61	1.82
R/G	1500	375	90.9	26.56	2.97
$\bar{p}$	20.0	10.0	5.0	27.0	0.9

FIGURE 3. Rise curves for the centre of gravity of 300 circular particles fluidized by lift (fluid viscosity = 1.0 poise, $G = 9.81/R$). The timescale for the slow rise at $\bar{p} = 0.9\,\mathrm{dyn\,cm^{-3}}$ has been compressed by 2; the real time corresponding say, to 50.01 is 100.02 s. The bed is said to be fully fluidized when the rise curves level off. The time to full fluidization is longer when the Reynolds number is smaller.

4. Fluidization of 300 circular particles

Here, we study the problem of lift of 300 solid circles in plane Poiseuille flow (figure 2) when $\rho_p = 1.01\rho_f, \rho_f = 1\,\mathrm{g\,cm^{-3}}$, $W = 12d$ and $d = 1\,\mathrm{cm}$ for viscosities $\eta = 1$, 0.2 and 0.01 poise (from light oil to water). The calculations are carried out in a periodic domain $L = 63d$ which is long enough to contain four or more of the waves of pressure which characterize fully fluidized beds of 300 particles. The period of the waves does not depend on the period of the computational cell, provided that the cell contains more than three waves. Initially, the circles are arranged in a square lattice in which the particles do not touch; they are separated by 0.05 cm when $\eta = 1$ and $\eta = 0.2$ poise, and by 0.1 cm when $\eta = 0.01$ poise. The height of the array is 5.25 cm and 5.35 cm.

Initially, the particle array is at rest and the fluid above is a developed Poiseuille flow; this kind of initial condition causes a faster saltation type of lift, like a dust storm in a sudden wind. The same final rise height can be obtained from different initial conditions.

We recall that the results of calculations may be generalized by computing the values of the shear Reynolds number $R = \dot{\gamma}_w d^2/\nu$ and the gravity number $G = d(\rho_p - \rho_f)g/\dot{\gamma}_w\eta$ defined in (2.3). The value $R_G = RG = \rho_f d^3(\rho_p - \rho_f)g/\eta^2 = 9.81/\eta^2$ is independent of $\dot{\gamma}_w$. The running index in our calculation is the pressure gradient $\bar{p}$; given η, this determines $R = \rho d^2 W\bar{p}/2\eta^2 = 6\bar{p}/\eta^2$.

4.1. *Case* 1: $\eta = 1$ *poise*, $R_G = 9.81$

Figure 3 shows the height of the centre of gravity of the 300 particles as a function of $R = 6\bar{p}$. We say that the bed height has attained its final fully fluidized value when the rise curve levels off. Average values of the bed height $\bar{H}$, the average velocity $\bar{U}\,\mathrm{cm\,s^{-1}}$ and angular velocity $\bar{\Omega}\,\mathrm{s^{-1}}$ at full inflation are given in table 1. The time taken for the

R	G	$\bar{p}$	$\bar{H}$	$\bar{U}$	$\bar{\Omega}$
5.4	1.82	0.9	3.01	2.09	0.28
16.2	0.61	2.7	3.54	9.55	1.026
24	0.41	4.0	4.00	18.62	1.75
30	0.33	5.0	4.17	25.63	2.25
60	0.16	10.0	4.69	55.60	3.85
120	0.08	20.0	5.24	119.76	4.90

TABLE 1. Data for the forward motion of a fluidized suspension of 300 particles after the bed has fully inflated and the average height $\bar{H}$ of all particles has stopped increasing ($\eta = 1.0$). $\bar{H} = \bar{H}_0 = 2.65d$ at $t = 0$. $\bar{U}$ and $\bar{\Omega}$ are the average velocity and angular velocity of the particles.

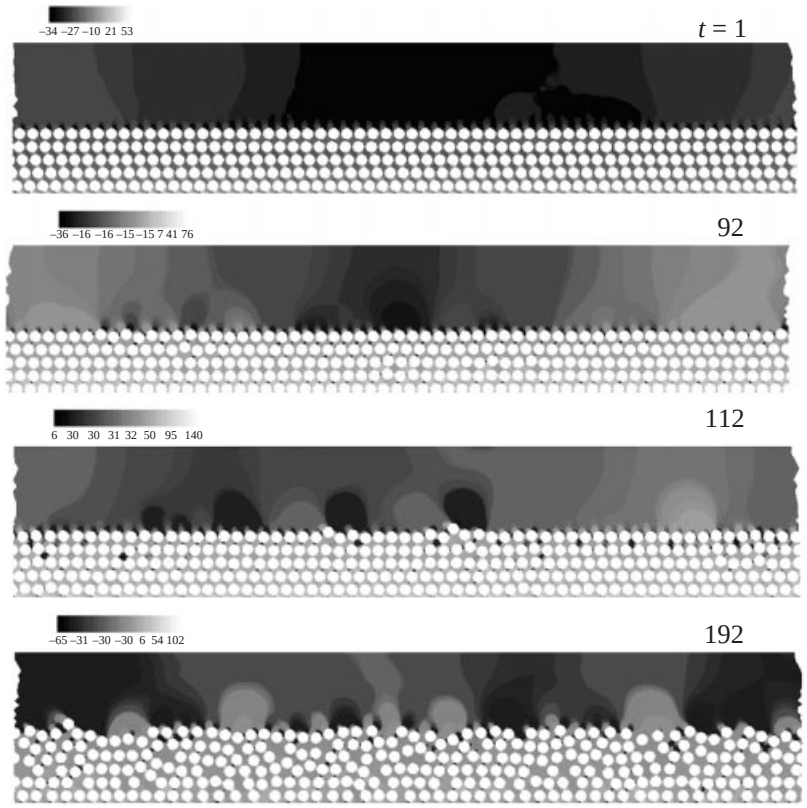

FIGURE 4. Snapshots of the fluidization of lift of 300 circular particles $\rho_p = 1.01\,\mathrm{g\,cm^{-3}}$ when $\eta = 1$ poise ($R = 5.4$, $G = 1.82$). The flow is from left to right. The grey scale gives the pressure intensity and dark is for low pressure. At early times, particles are wedged out of the top layer by high pressure at the front and low pressure at the back of each and every circle in the top row. The vertical stratification of pressure at early times develops into a 'periodic' horizontal stratification, a propagating pressure wave. The final inflated bed has eroded, rather tightly packed at the bottom with fluidized particles at the top.

centre of gravity to reach its fully fluidized value increases as the Reynolds number R decreases. Figures 4 to 7 show snapshots of the evolution of the bed to full fluidization at values of R and G given in the caption to figure 3.

Animations for these snapshots can be found at our URL *http://www.aem.umn.edu/*

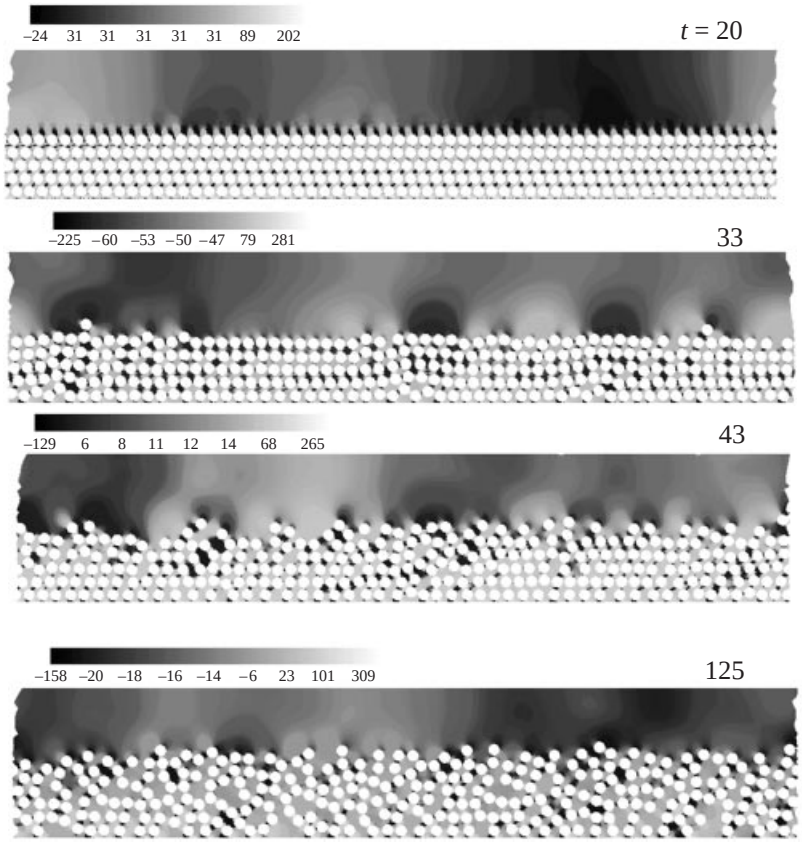

FIGURE 5. Fluidization of 300 particles ($R = 16.2$, $G = 0.61$). The conditions are the same as in figure 4 except that the lift forces are greater, leading to a more complete and faster fluidization.

Solid-Liquid_Flows. The snapshots are decorated by shades of grey coded to reveal the distribution of dynamic pressure ($\bar{p}$ in (3.1)); dark means low pressure. Figures 8 and 9 show the pressure at different cross-sections of the channel for $R = 120$ at an early time $t = 0.9$ s and when the suspension is fully fluidized at $t = 27$ s. At early times, the pressure is stratified vertically, but not horizontally; at the later time, the pressure is stratified horizontally and not vertically.

In figures 8 and 9 we plotted the distribution of pressures at an early and late time when $R = 120$ and $G = 0.08$. The figures show that the vertical stratification of pressure at an early time evolves to waves of pressure which are associated with propagating number density or voidage waves.

4.2. *Case* 2: $\eta = 0.2$ *poise*, $R_G = 245$

Figure 10 shows the height of the centre of gravity of the 300 particles as a function of $R = 6\bar{p}/\eta^2$. The interpretation of figure 10 is the same as figure 3. Average values of the bed height $\bar{H}$ cm, velocity $\bar{U}$ cm s^{-1}, and angular velocity $\bar{\Omega}$ s^{-1} at full fluidization are given in table 2. Snapshots of the evolution to full fluidization are shown in figures 11 and 12.

The description in the caption of figure 4 applies also to figures 11 and 12 except that the particles are more mobile when the viscosity of the fluid is smaller. The particle laden region at $t = 25$ s in figure 11, and $t = 1.98$ s in figure 12 is separated

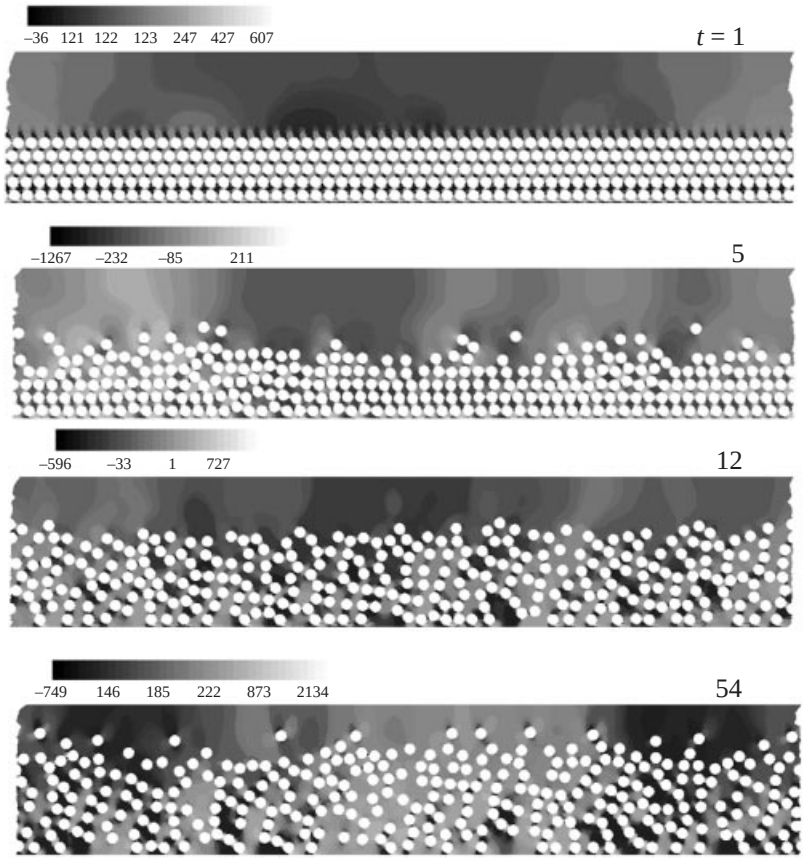

FIGURE 6. Fluidization of 300 particles ($R = 60$, $G = 0.16$). The conditions are as in figure 4. The ratio $R/G = \dot{\gamma}_w^2 d/(g\Delta\rho/\rho)$ measures the ratio of lift to buoyant weight. Here the ratio is very large, leading to a fast and complete fluidization; the entire bed has eroded.

from the particle-free region by an 'interface' which propagates like an interfacial wave. This interface disappears at a higher $R = 450$, figure 12 for $t > 2.7$ s, because the stronger lift forces push wave crests into the top of the channel; however, the pressure and associated void fraction wave persists.

The pressure wave at $t_0 = 4.204$ s for the case ($\eta = 0.2$, $R = 450$) in figure 12 is analysed in figure 13. The period of this wave is $T = 0.56$ s and its wavelength is 16 cm. The pressure wave is associated with a wave of solids fraction which could also be described as the passage of internal wave crests and troughs.

Figures 14 and 15, like figures 8 and 9, show the evolution of dynamic pressure from an essentially vertical stratification at early time ($t = 0.1$ s) to propagating horizontal waves in the fully developed suspension at $t = 4.95$ s.

4.3. *Case* 3: $\eta = 0.01$ *poise*, $R_G = 9.81/\eta^2 = 9.8 \times 10^4$

Figure 16 gives the height of the centre of gravity of 300 particles in water as a function of $R = 6\bar{p}/\eta^2 = 6 \times 10^4 \bar{p}$. The interpretation of figure 16 is the same as figure 3. Snapshots of the evolution to full fluidization are shown in figures 17 and 18.

The evolution to full fluidization is accomplished by pressure waves. For low Reynolds numbers the bed expansion is small; the snapshot at $t = 116$ s in figure 17 is an example of bed expansion in water at low R. The bed has expanded by the

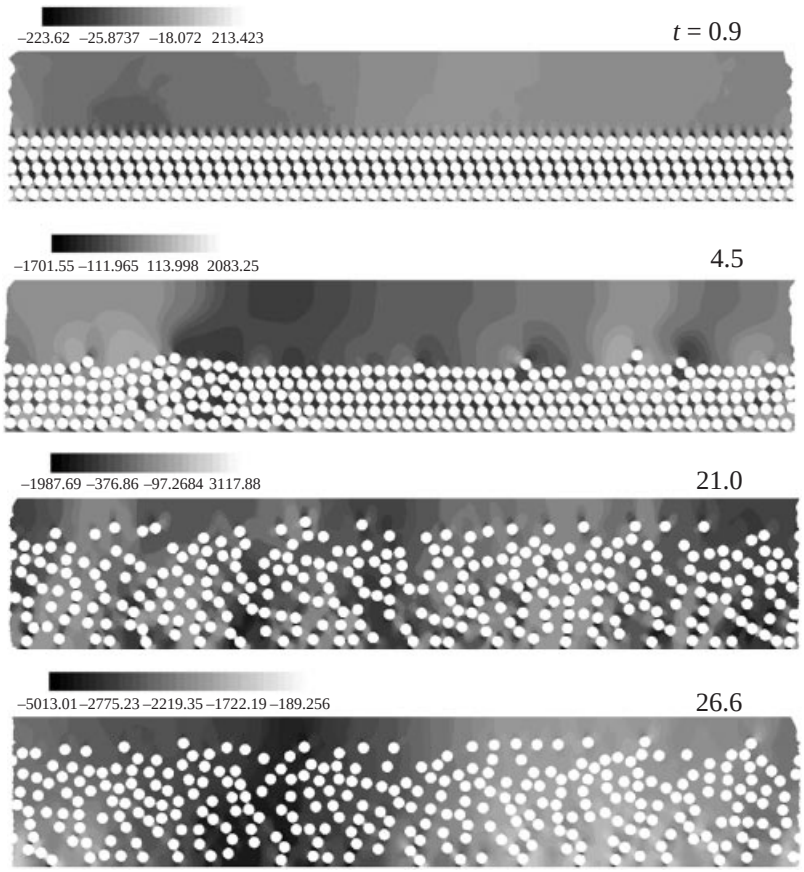

FIGURE 7. Fluidization of 300 particles ($R = 120$, $G = 0.08$). The conditions are the same as in figures 4 and 6 but the ratio of life to buoyant weights is greater and the fluidization is faster and the particle mass centre rises higher than in the previous fiugres.

development of voids and dislocations near the top of the bed; only a few particles are fluidized. The bed is not severely eroded.

Fluidization in water at high Reynolds numbers is greatly different. The fully fluidized bed shown at $t = 0.46$ s in figure 18 is completely eroded. The evolution of the fluidized suspension is driven by a propagating pressure wave, which is in one-to-one correspondence with the propagation of voids. At $t = 0.27$ s, before the bed has fully fluidized, these voids coincide with wave troughs.

Figures 19 and 20 show how the dynamic pressure p develops as the bed evolves to full fluidization. For this case, $t = 0.1$ s is not an early time; the periodic pressure pulses which drive particles into suspension have already developed.

Figure 21 focuses on the wave properties of the evolving fluidization of 300 particles in water when $R = 1200$. The $t = 40$ s panel of figure 17 shows a propagating and nearly spatially periodic wave of particles. Waveforms for the dynamic pressure p, the vertical velocity V, and the horizontal velocity U are shown.

4.4. *Inertial mechanism of fluidization*

We studied the fluidization of 300 circular particles in a Poiseuille flow. Initially, the particles are arranged in a cubic array filling nearly half the channel. The flow breaks

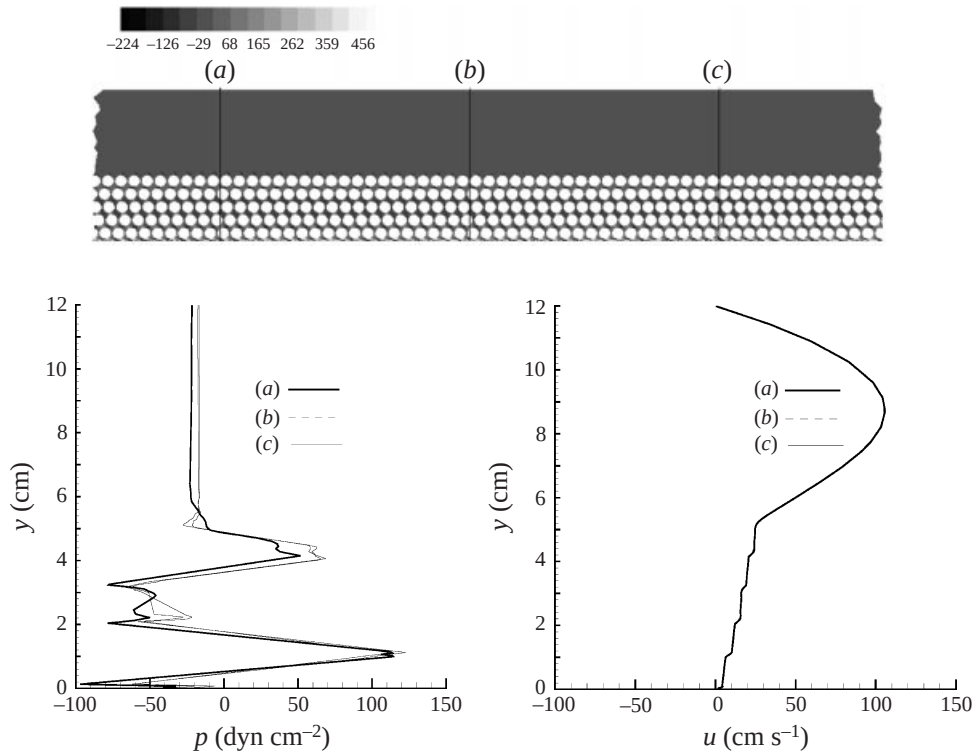

FIGURE 8. Distribution of dynamic pressure p and streamwise velocity u at an early time ($t = 0.9$ s) when $R = 120$, $G = 0.08$ (cf. figure 7) at different cross-sections of the channel. The dynamic pressure is stratified vertically but not horizontally. The rows of particles slide relative to one another moving like rigid bands separated by liquid.

the cubic array and inflates the bed by pumping liquid into the bed. The pressures that develop in the bed can levitate the particles. Bed inflation may be divided into two regimes; an eroded bed in which only the top rows of the bed have been inflated, and a fully fluidized bed in which all of the particles are supported by lift forces from the fluid flow. The pumping of liquid into the bed at the earliest times appears to be a universal inertial effect associated with potential flow around spheres and circles. This inertial effect produces high pressure at the front and low pressure at the back side of each circle in the top row of the array. This produces a pressure differential front to back, creating a flow into and out the bed, which dislodges particles from the top row. Further fluidization is driven by the development of a periodic wave of pressure and number density which are clearly evident in the snapshots of the bed evolution.

Apart from aspect and density ratios, the dimensionless equations are fully specified by the values of a shear Reynolds number $R = \dot{\gamma}wd^2/\nu$ and a gravity number $G = d(\rho_p - \rho_f)g/\dot{\gamma}_w\eta$ and the number of particles in the cell. The ratio R/G is independent of η and can be viewed as the ratio of lift to buoyant weight whereas the product RG is independent of $\dot{\gamma}_w$ and can be regarded as the ratio of buoyant to viscous damping; there is rapid bouncing around when RG is large, and high lifts, high average height and very inflated beds when R/G is large. A summary of the average height, velocity and angular velocity of the particles in the fully inflated beds for $\eta = 1$, 0.2 and 0.01 poise are presented in tables 1–3.

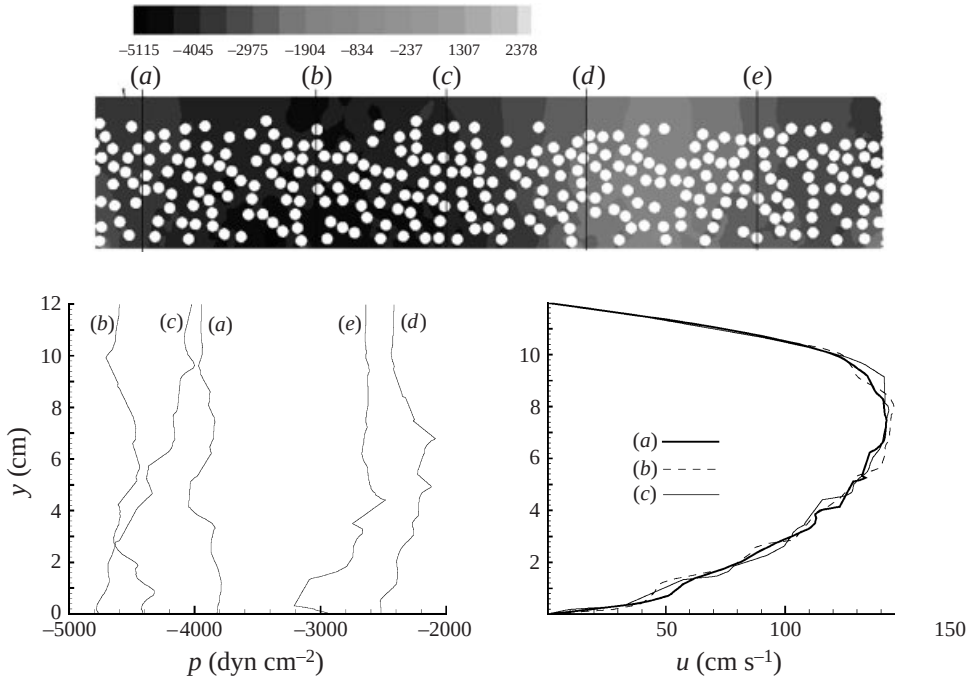

FIGURE 9. Distribution of dynamic pressure p and streamwise velocity u after full fluidization ($t = 27$ s) when $R = 120$, $G = 0.08$. The pressure p is stratified horizontally and not vertically; pressure pulses propagate horizontally.

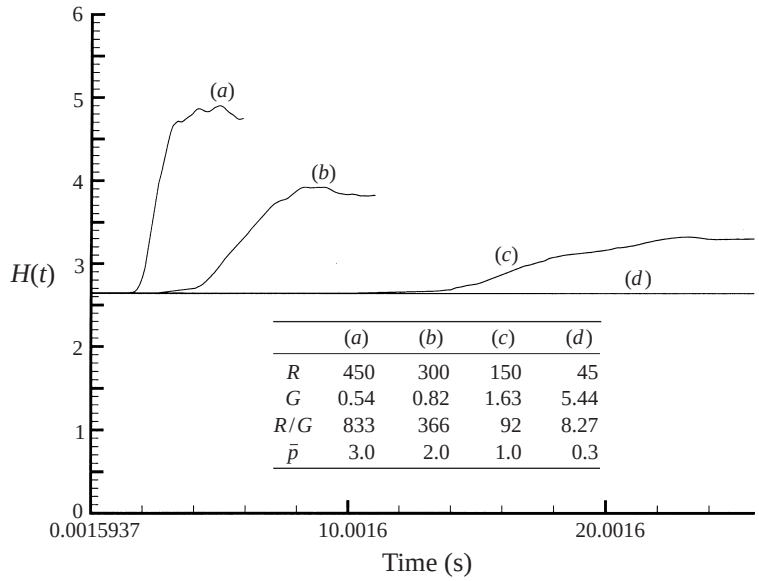

	(a)	(b)	(c)	(d)
R	450	300	150	45
G	0.54	0.82	1.63	5.44
R/G	833	366	92	8.27
$\bar{p}$	3.0	2.0	1.0	0.3

FIGURE 10. Rise curves for the centre of gravity of 300 circular particles fluidized by lift (fluid viscosity = 0.2, $RG = 9.81/\eta^2 = 245$.) $\bar{p}$ is in dyn cm^{-3}. The bed is fully fluidized when the rise curves level off. The time to full fluidization is longer when the Reynolds number is smaller. The time to full fluidization is faster when $\eta = 0.2$ than when $\eta = 1$ (figure 3). The time is scaled down by 5 and the centre of gravity of the particles will eventually rise when $(R, \bar{p}) = (45, 0.3)$.

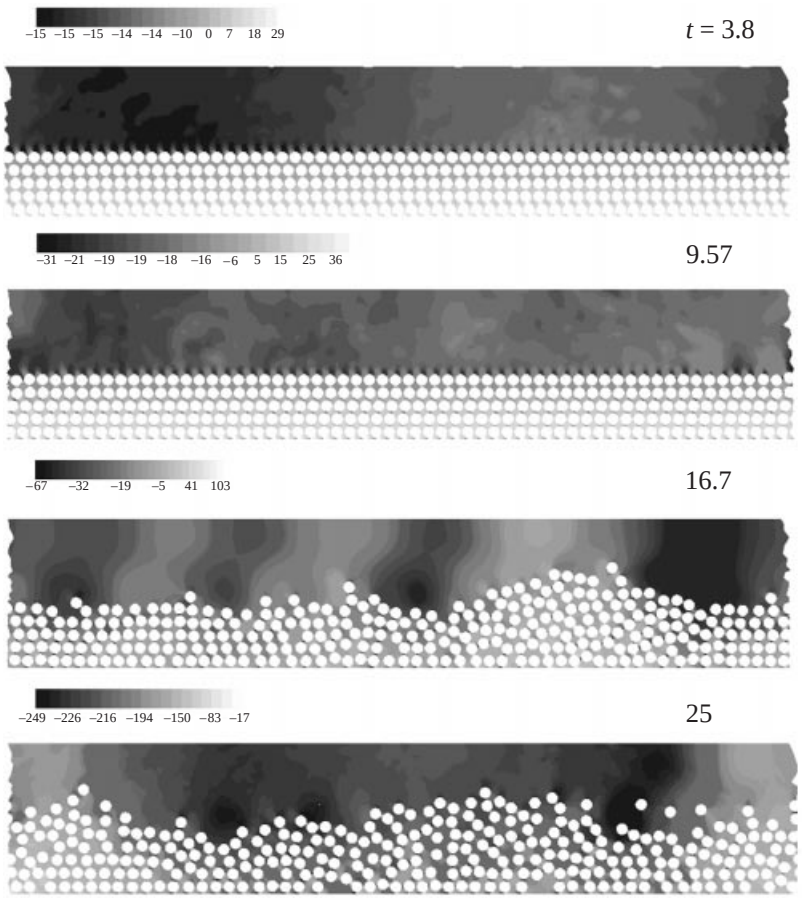

FIGURE 11. Fluidization of 300 particles ($\eta = 0.2$ poise, $R = 150$, $G = 1.63$). The final state of the fluidization at $t = 25$ s has not fully eroded. The particles that lift out of the bed can be described as saltating. A propagating 'interfacial' wave is associated with the propagating pressure wave at $t = 250$ s.

R	G	$\bar{p}$	$\bar{H}$	$\bar{U}$	$\bar{\Omega}$
45	5.44	0.3	2.64	3.17	0.42
150	1.63	1.0	3.30	10.75	1.25
300	0.82	2.0	3.82	22.98	2.43
450	0.54	3.0	4.75	34.15	2.02

TABLE 2. Data for the forward motion of a fluidized suspension of 300 particles after the bed has fully inflated and the average height $\bar{H}$ of all particles has stopped increasing ($\eta = 0.2$). $\bar{H} = \bar{H}_0 = 2.65d$ at $t = 0$. $\bar{U}$ and $\bar{\Omega}$ are the average velocity and angular velocity of the particles.

4.5. *Model of slip velocity*

In the modelling of solid–liquid flows, the slip velocity is an important but sometimes ambiguous quantity. For single-particle lift studies, the slip velocity is defined as the difference between the fluid velocity at the particle centre when there are no particles and the particle velocity. When there are many particles, other possibilities

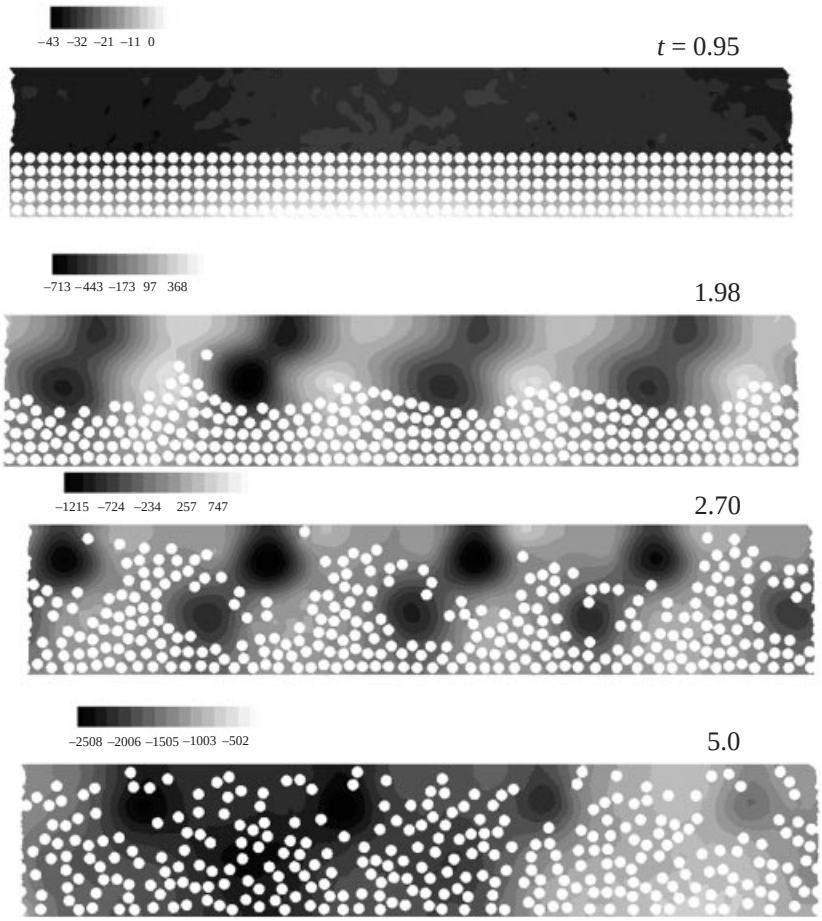

FIGURE 12. Fluidization of 300 particles ($\eta = 0.2$ poise, $R = 450$, $G = 0.54$). The flow is from left to right. The particles can be lifted to the top of the channel.

become viable. For example, in the well-known drift flux model (see Wallis 1969) drift velocities are defined as the difference between the component velocities and the composite velocity. This kind of definition is useful when there is a large difference in a average solid and liquid velocity. In sedimenting suspensions and in suspensions fluidized by drag, these large differences arise from the back flow which is absent in suspensions fluidized by lift. For such suspensions, the concept of 'slip' requires analysis.

Joseph (2000) proposed a model problem for plane Poiseuille flow defined in figure 22 in which we replace the circle of diameter d with a long rectangle whose short side is d, the rectangle is so long that we may neglect effects of the ends of the cylinder at sections near the cylinder centre. The midplane of the cylinder is a distance y_1 from the bottom wall and

$$y_1 > \tfrac{1}{2}d, \quad W - y_1 > \tfrac{1}{2}d. \tag{4.1}$$

When no particle is in the flow

$$u = \frac{\bar{p}}{2\eta}\, y(W - y). \tag{4.2}$$

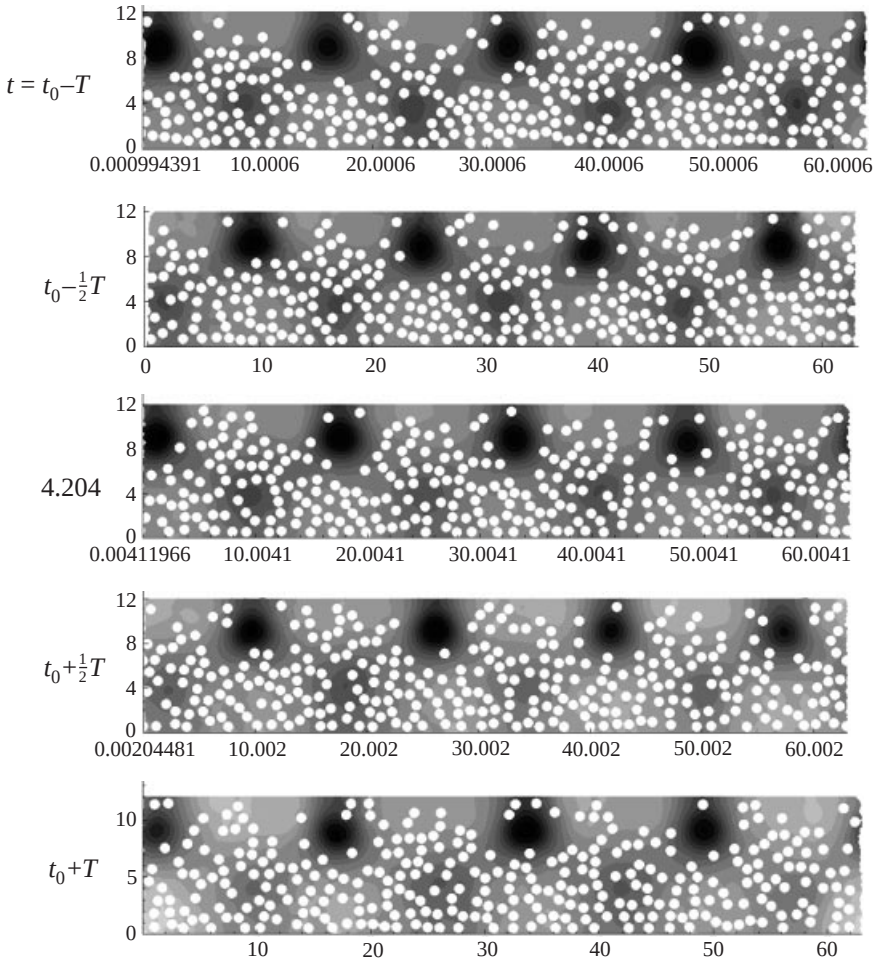

FIGURE 13. Propagation of the pressure wave centred at $t_0 = 4.204$ s ($\eta = 0.2$ poise, $R = 450$) shown in figure 12. The period T of this wave is $T = 0.56$ s and its wavelength is 16 cm.

The long particle is moved forward by shear from the Poiseuille flow at a speed U_p which we shall obtain from the particles equation of motion (4.9) for steady flow. When $0 \leqslant y \leqslant y_1 - \frac{1}{2}d$, we find

$$u = \frac{\bar{p}}{2\eta} y[y_1 - \tfrac{1}{2}d - y] + \frac{U_p y}{y_1 - \frac{1}{2}d}. \tag{4.3}$$

When $y_1 + \frac{1}{2}d \leqslant y \leqslant W$, we have

$$u = \frac{\bar{p}}{2\eta}(y - W)[y_1 + \tfrac{1}{2}d - y] + \frac{U_p(y - W)}{y_1 + \frac{1}{2}d - W}. \tag{4.4}$$

For the force balance, consider the long rectangle whose long side is L and short side is d, as in figure 22. The cylinder moves forward with steady velocity U_p. The cylinder is impelled forward by the pressure force $(p_1 - p_2)d$ and is resisted by a shear

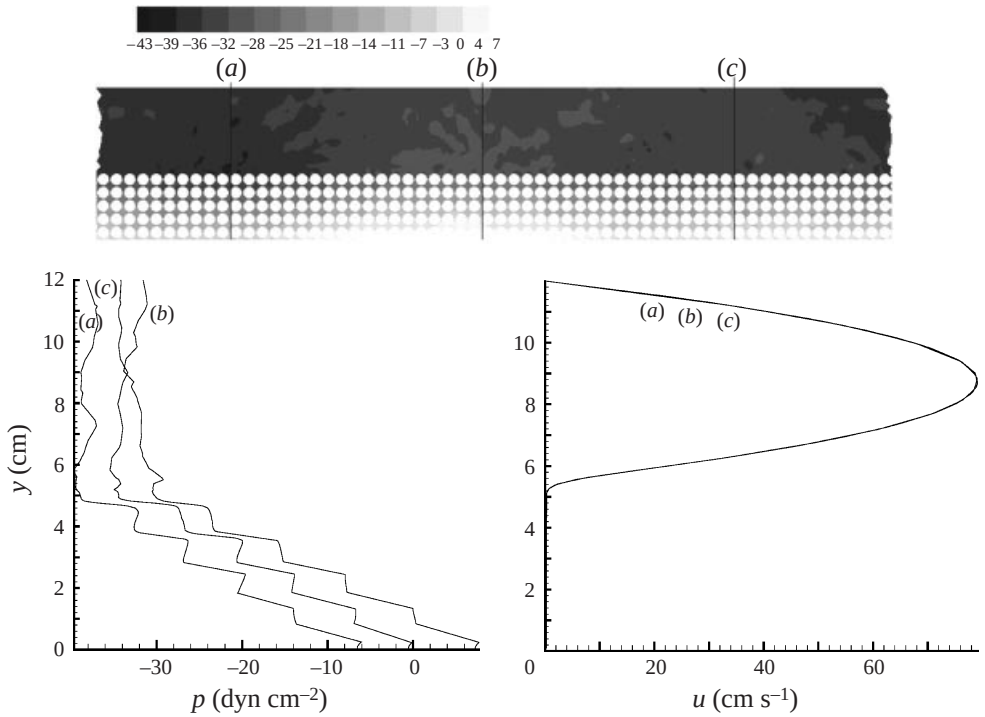

FIGURE 14. Distribution of dynamic pressure p and streamwise velocity u at $t = 0.1$ s when $R = 350$, $\eta = 0.2$ poise. The distribution is vertical. This kind of distribution is typical of the earliest times. The vertical steps show how the fluid supports rows of particles. The particles move forward together, with only a small velocity.

force from the fluid motion

$$(\tau_{xy}|_{y_1+d/2} - \tau_{xy}|_{y_1-d/2})L = \eta \left(\left.\frac{\mathrm{d}u}{\mathrm{d}y}\right|_{y_1+d/2} - \left.\frac{\mathrm{d}u}{\mathrm{d}y}\right|_{y_1-d/2} \right) L. \tag{4.5}$$

Equating the pressure and shear forces, after dividing by L and writing $(p_1 - p_2)/L = \bar{p}$, we obtain

$$\bar{p}d = \eta \left.\frac{\mathrm{d}u}{\mathrm{d}y}\right|_{y_1-d/2} - \eta \left.\frac{\mathrm{d}u}{\mathrm{d}y}\right|_{y_1+d/2}, \tag{4.6}$$

where

$$\left.\frac{\mathrm{d}u}{\mathrm{d}y}\right|_{y_1+d/2} = -\frac{\bar{p}}{2\eta}(y_1 + \tfrac{1}{2}d - W) + \frac{U_p}{y_1 + \tfrac{1}{2}d - W}, \tag{4.7}$$

$$\left.\frac{\mathrm{d}u}{\mathrm{d}y}\right|_{y_1-d/2} = -\frac{\bar{p}}{2\eta}(y_1 - \tfrac{1}{2}d) + \frac{U_p}{y_1 - \tfrac{1}{2}d}. \tag{4.8}$$

After combining the last three equations we find that

$$U_p = \frac{\bar{p}}{2\eta} \left\{ \frac{W + d}{W - d}(y_1 - \tfrac{1}{2}d)(W - y_1 - \tfrac{1}{2}d) \right\}. \tag{4.9}$$

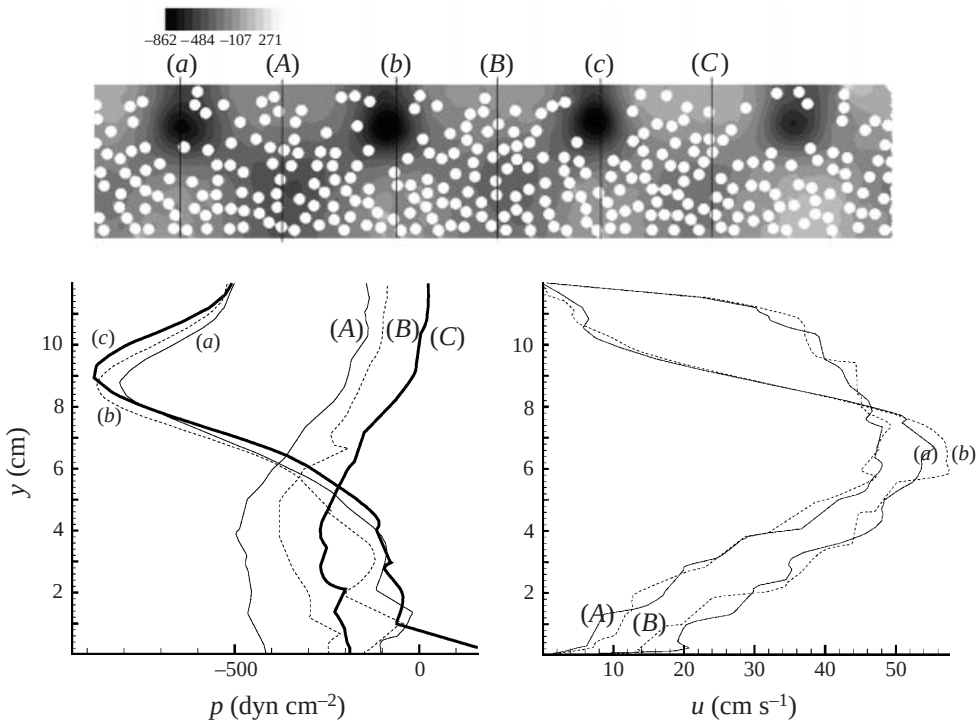

FIGURE 15. Distribution of dynamic pressure p and streamwise velocity u at $t = 4.95$ when $R = 350$, $\eta = 0.2$ poise (see figure 12). The pressure and velocity distribution can be associated with 'crest' and 'trough' propagating void fractions.

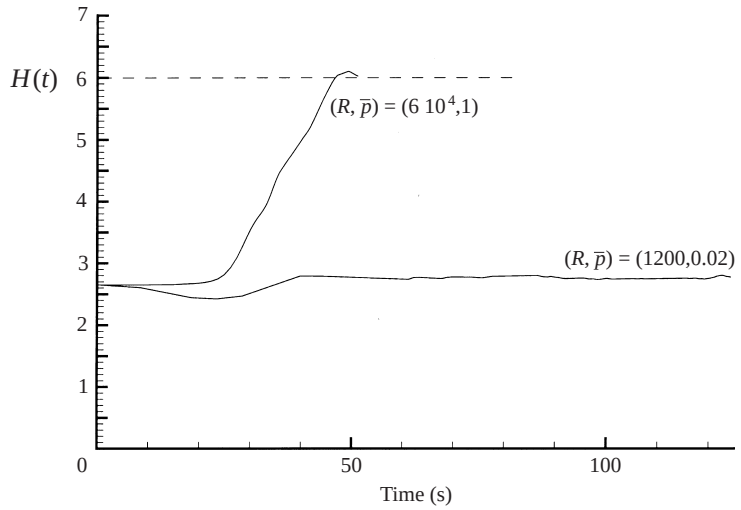

FIGURE 16. Rise curves for the centre of gravity of 300 circular particles fluidized by lift ($\eta = 0.01$, $RG = 9.81/\eta^2 = 9.81 \times 10^4$). $\bar{p}$ is in dyn cm^{-3}. The timescale for the fast rise at $\bar{p} = 1.0$ has been expanded by 100; the real time corresponding, say, to 50 is 0.5 s. The rise to full fluidization is very rapid and at full fluidization the mass centre of the particles is closer to the top than to the bottom wall. The bed inflation at $R = 1200$ is modest; at early times the position of the mass centre actually decreases because the circles are more efficiently packed (hexagonally, rather than cubically packed at $t = 27$).

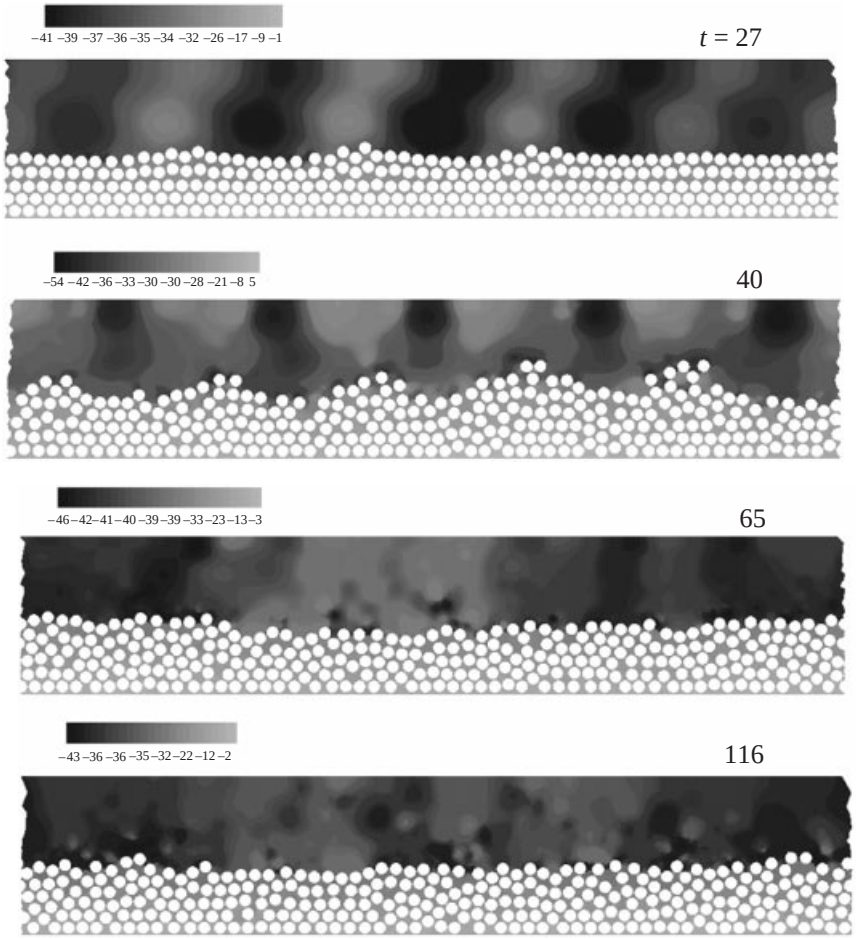

FIGURE 17. Fluidization of 300 particles ($\eta = 0.01$ poise, $R = 1200$, $G = 81.75$). The flow is from left to right. This is a 'relatively' heavy suspension with a smaller value of R/G. At $t = 27$ the flow packs the initial cubic array more closely into a hexagonal array and the mean bed height drops. The final fluid condition for $t > 116$ is mildly inflated, more closely packed at the bottom than the top.

R	R_g	$\bar{p}$	$\bar{H}$	$\bar{U}$	$\bar{\Omega}$
1200	81.75	0.02	2.77	0.63	0.04
6×10^4	1.64	1.0	6.02	116.20	4.50

TABLE 3. Data for the forward motion of a fluidized suspension of 300 particles after the bed has fully inflated and the average height $\bar{H}$ of all particles has stopped increasing ($\eta = 0.01$). $\bar{H} = \bar{H}_0 = 2.65d$ at $t = 0$. $\bar{U}$ and $\bar{\Omega}$ are the average velocity and angular velocity of the particles.

When $d \to 0$,

$$U_p \to \frac{\bar{p}}{2\eta} y_1(W - y_1), \tag{4.10}$$

which is the value $U(y_1)$ of the fluid velocity given by (4.2).

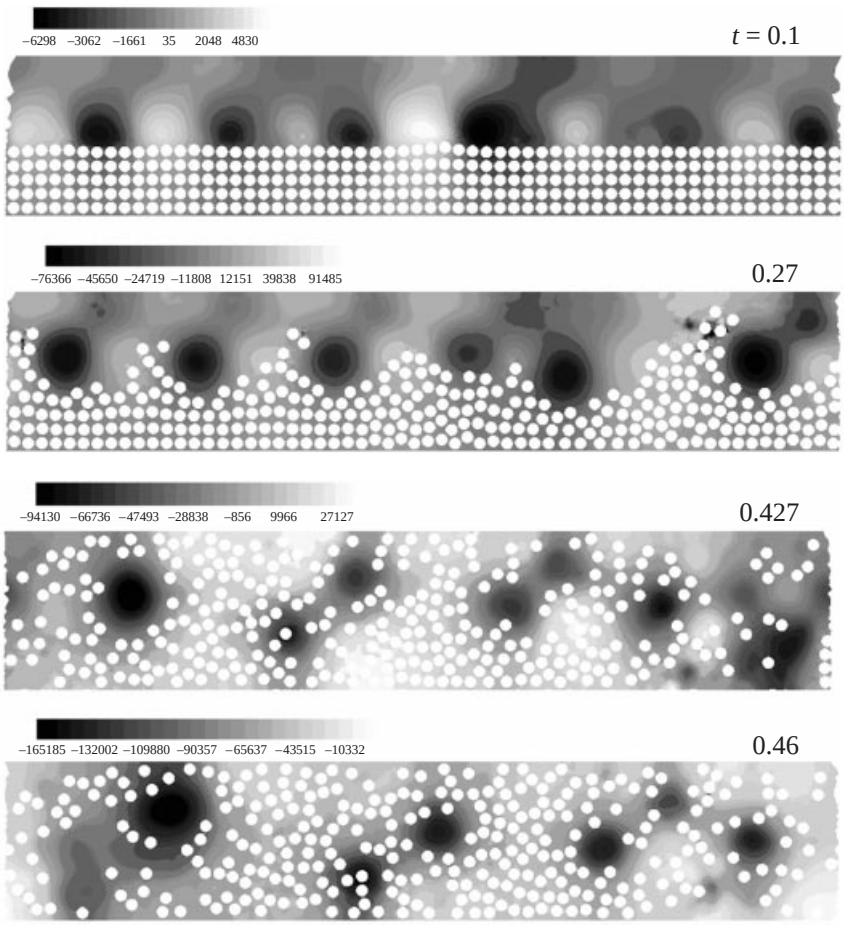

FIGURE 18. Fluidization of 300 particles in water ($\eta = 0.01$ poise, $R = 6 \times 10^4$, $G = 1.64$). This is a 'relatively' light suspension with a much larger value of R/G. Particles fluidize easily; the mean bed height is higher than midchannel.

We next evaluate the slip $U(y_1) - U_p$ forming the ratio

$$\frac{U_p}{U(y_1)} = \left(\frac{W+d}{W-d}\right)\left(\frac{y_1 - \frac{1}{2}d}{y_1}\right)\left(\frac{W - y_1 - \frac{1}{2}d}{W - y_1}\right). \tag{4.11}$$

To show that $U_p/U(y_1)$ is less than 1 when $d > 0$, we note that

$$(W-d)y_1(W-y_1) - (W+d)(y_1 - \tfrac{1}{2}d)(W - y_1 - \tfrac{1}{2}d) = (y_1 - W/2)^2 + \tfrac{1}{8}d(W-d) > 0.$$

In our simplified model, the fluid velocity is larger than the particle velocity in steady flow and the lag increases as the particle diameter increases. Small particles follow the fluid with vanishing lag.

This calculation suggests that the presence of even one particle can produce a global change of the fluid velocity. This kind of global change can be generated by circles, as is shown in figures 23 and 24. The velocity profiles far upstream and downstream of the particle tend to undisturbed values. The effect of particle rotation is to diminish the effect of the particle on the fluid motion. Our long particle cannot rotate but we could express an effect of rotation by allowing for a shear profile, less

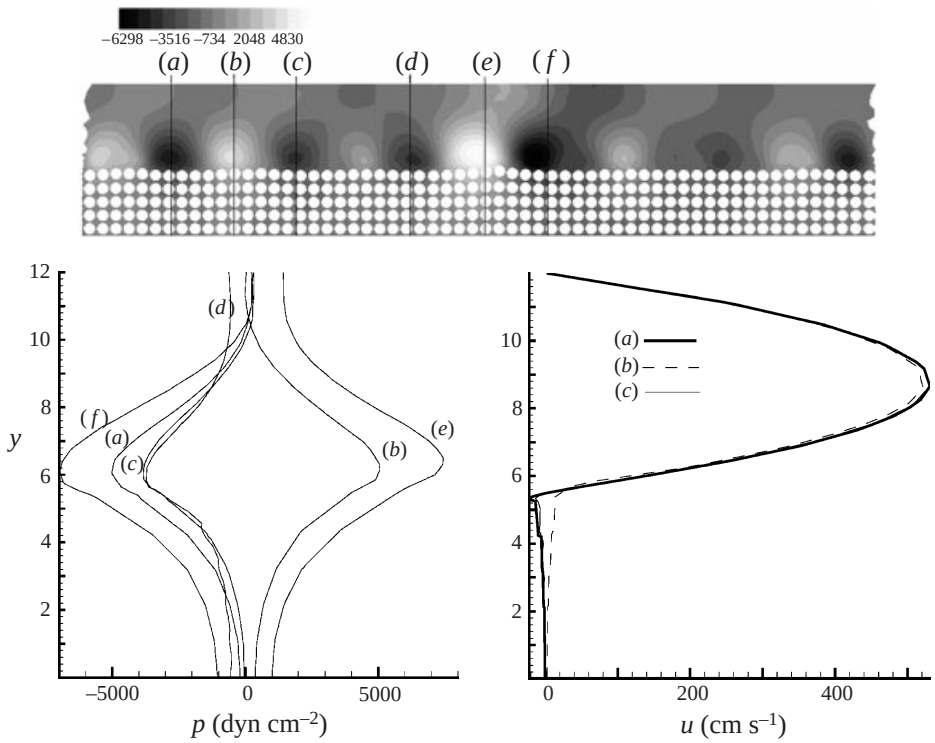

FIGURE 19. Distribution of dynamic pressure p and streamwise velocity u at $t = 0.1$ s for the fluidization of 300 particles in water when $R = 6 \times 10^4$ (see figure 18). In this case, $t = 0.1$ s is not an early time; the propagating pressure wave has already developed, but it does not yet have a big effect on the velocity distribution.

than the shear in the unperturbed fluid, in the long body as if it were a very viscous fluid. The shear in the very viscous fluid would be greater than the zero shear of the solid and less than the shear in the undisturbed flow. The difference between the shear in the undisturbed fluid and the very viscous fluid can be viewed as representing the angular slip velocity. The 'no shear' solid corresponds to a circular particle for which rotation is suppressed.

The presence of more than one particle produces yet more lag globally and the best way to see the change is to compare the profile with the undisturbed flow. In figure 25 we have used tecplot to plot profiles at 6 different sections of the flow of 300 particles at $\bar{p} = 20\,\mathrm{dyn\,cm^{-3}}$, $t = 28$ s identified by vertical lines in figure 7. The open circles give the velocity at fluid points. The straight line segments pass through particles which are rotating. There is no slip velocity in such a plot; the velocity is continuous through the particle.

In figure 26 we plotted the 10 average fluid velocities as a function of y. They are obtained by averaging fluid velocities at about 1000 points of the x-coordinate at a fixed y. These averages are shown as 10 black circles. A scatter plot of particle velocities is shown and a polynomial fit to this scatter plot is given as a light solid. There does not seem to be a large difference between the average fluid velocity and the average solid velocity defined in this way. On the other hand, the difference between the composite fluid–solid velocity and the particle free Poiseuille flow profile is dramatic.

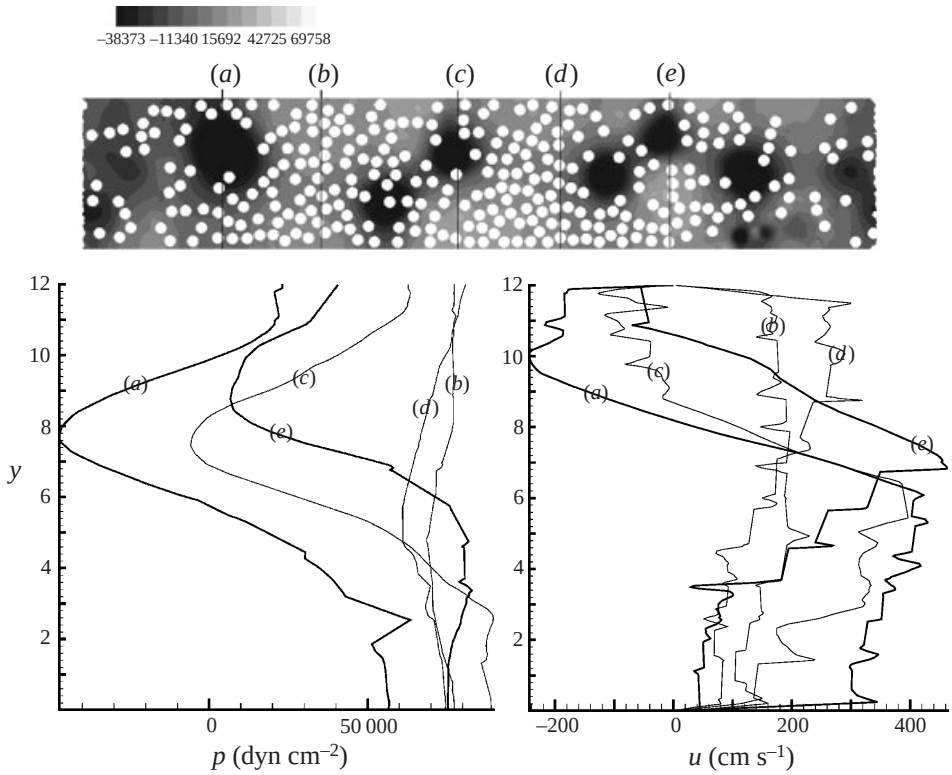

FIGURE 20. Distribution of dynamic pressure p and streamwise velocity u at $t = 0.46$ s (see figure 18). The pressure and velocity wave coincide with the propagation of internal waves of void fractions.

The data shown in figure 26 suggest that one of the main effects of particles in a fluid is to radically reduce the velocity of the composite. Each particle produces a drag on the fluid in a freely moving suspension. The effect of such a distributed drag is equivalent to some form of effective viscosity. Algorithms for the construction of such effective viscosities would find many important applications. Unfortunately, the empirical forms of effective viscosity functions which work well for uniform fluidized and sedimenting suspensions work much less well for sheared suspensions.

For comparison, we calculated velocity profiles using a two-fluid effective viscosity theory. We suppose that the particle-laden region is an effective fluid with an effective viscosity and an effective density, though the effective density is not required for the calculation to follow. The selection of the region occupied by the fluid–solid mixture is somewhat arbitrary. We suppose that the mixture has a uniform volume fraction under a flat interface of height $2\bar{H}$, where $\bar{H}$ is the mean height. The volume fraction is obtained as $300\pi d^2/8\bar{H}L$ where $d = 1$ cm and $L = 63$ cm. Two highly regarded expressions for the effective viscosity of a uniform suspension of spheres of volume fraction ϕ are:

$$\eta_m = \eta_f/(1 - \phi/A)^2, \quad A = 0.638, \tag{4.12}$$

which is due to Kataoka *et al.* (1978) into two dimension and

$$\eta_m = \eta_f(1 + 2.5\phi + 10.05\phi^2 + 0.00273\mathrm{e}^{16.6\phi}) \tag{4.13}$$

which is due to Thomas (1965). These expressions were obtained from experiments

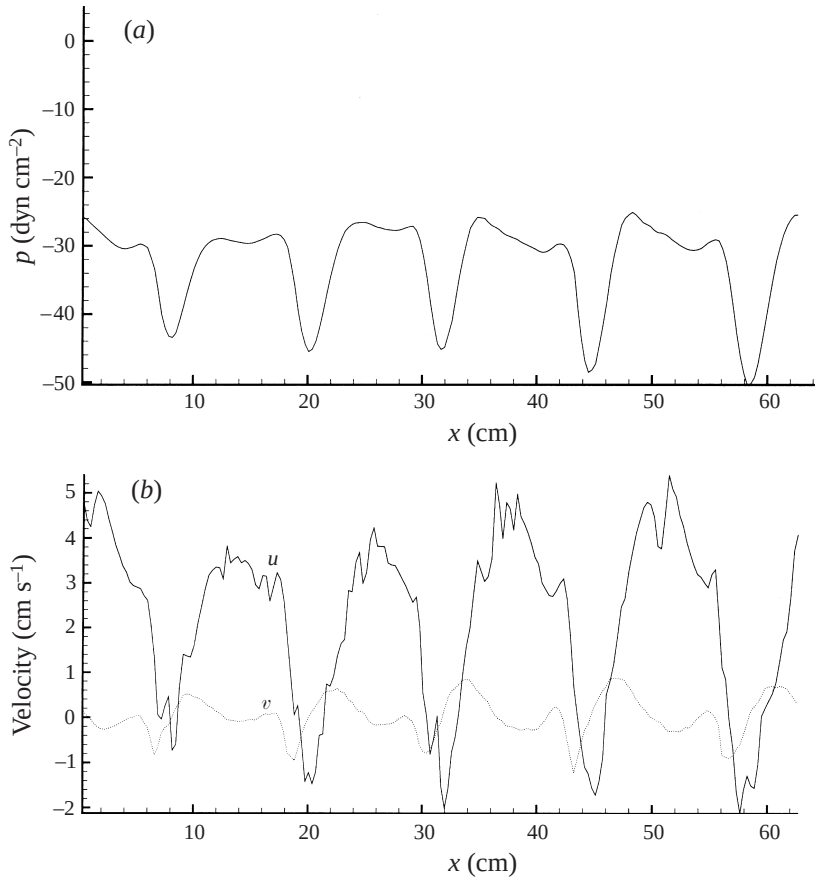

FIGURE 21. (*a*) Distribution of dynamic pressure p, (*b*) vertical velocity v and horizontal velocity u in water near the upper wall ($y = 11$ cm) at $t = 40$ when $R = 1200$, $G = 81.75$, see figure 17). These spatially periodic waves propagate.

and may not apply in two dimensions. We used $A = A_{2D} = 0.8328$ which scales A into two dimension in the ratio of close-packed hexagonal packings in two and three dimensions, $A_{2D} = (0.907/0.740)A_{3D}$. The effective theory is a two-fluid stratified Poiseuille flow satisfying the following equations

$$\bar{p} = \eta_f \frac{\partial^2 u_f}{\partial y^2} \quad \text{for} \quad y \geqslant h, \quad \bar{p} = \eta \frac{\partial^2 u_m}{\partial y^2} \quad \text{for} \quad y \leqslant h, \tag{4.14}$$

where $h = 2\bar{H}$ is the interface between the pure fluid and the mixture. At the boundary,

$$u_f(W) = 0.0, \quad u_m(0) = 0.0,$$

and the velocity and shear stress are continuous on $y = h$;

$$u_f(h) = u_m(h),$$

$$\eta_f \frac{\partial u_f}{\partial y}(h) = \eta \frac{\partial u_m}{\partial y}(h). \tag{4.15}$$

The comparison of the effective theory corresponding to (4.12) and (4.13) with the numerical simulation is exhibited in figure 26. The agreement between the effective

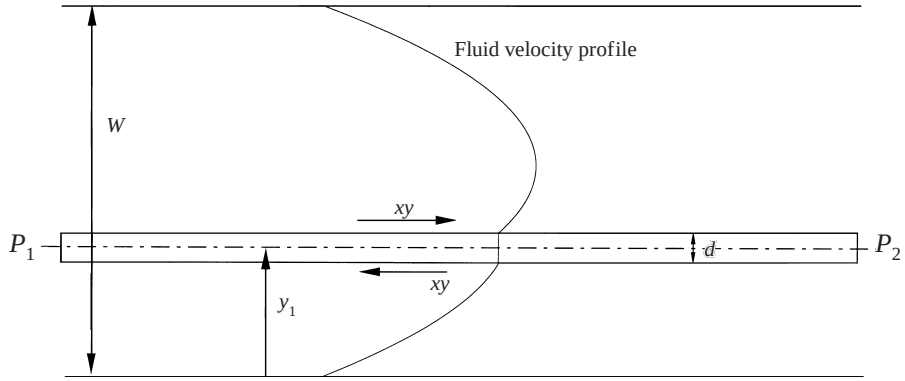

FIGURE 22. Forces on long particle in a steady Poiseuille flow.

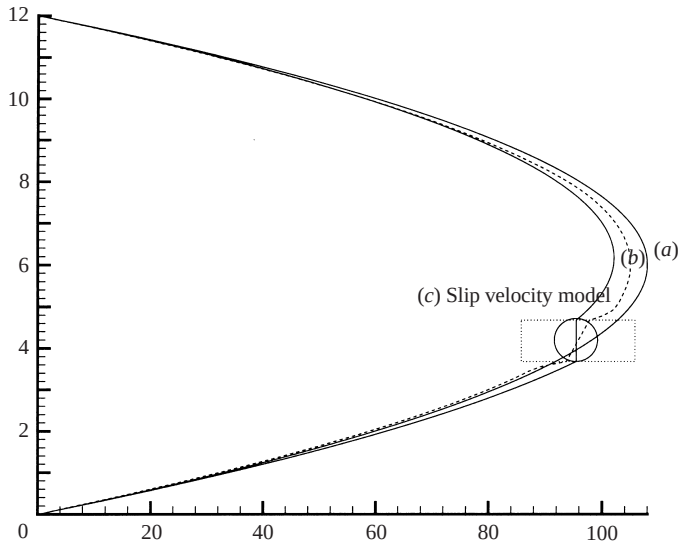

FIGURE 23. Velocity profiles for three different solutions with $W = 12\,\text{cm}$, $d = 1\,\text{cm}$, $\eta = 0.2\,\text{poise}$ and $\bar{p} = 1.2\,\text{dyn}\,\text{cm}^{-3}$. (*a*) Undisturbed Poiseuille flow, (*b*) DNS one circular particle $h_e = 4.18\,\text{cm}$ (see table 1), (*c*) model problem corresponding to figure 22 with $y = 4.18\,\text{cm}$. The model reduces the velocity much more because the particle is long and because it does not rotate.

theory and the simulation is far from perfect, but there is agreement within a large tolerance. However, the effective theory has several defects which must be overcome before it can be used to model the slurry. First and foremost, the theory requires that h be specified; here, from the simulation, a second problem is that the effective viscosity for uniform suspension need not be a good representation of sheared suspension. It is certain the effective density of the slurry must enter into the height of the fluidized slurry in ways that we do not yet understand.

The small difference between the spatially averaged fluid and solid velocities cannot be said to be clearly evident at all positions on a cross-section. It is our position that a positive slip velocity is required to support the buoyant weight of particles. In fact, we would expect that the difference between the particle weight and the composite density $\bar{\rho}(\phi) = \rho_p\phi + \rho_f(1-\phi)$ is a factor in the unknown formula for the lift on a particle in a swarm of volume fraction ϕ. In the present case,

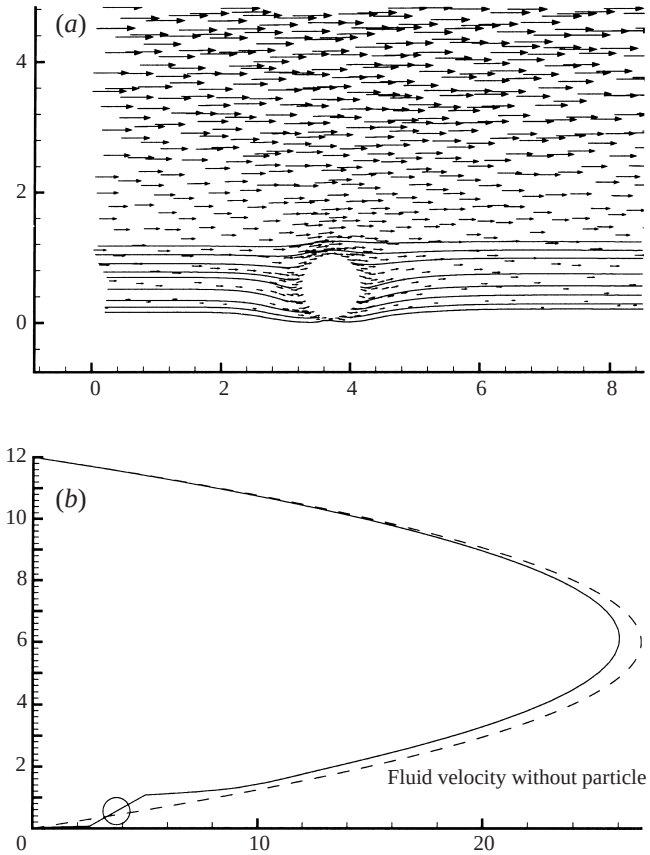

FIGURE 24. Velocity for the steady flow of a levitated particle near the wall ($R = 45$, $G = 5.4$, $\eta = 0.2$, $\bar{p} = 0.3$; see table 2). (*a*) Velocity vector and streamlines, (*b*) velocity profile on the vertical line through the particle centre.

$\rho_p - \bar{\rho}(\phi) = (\rho_p - \rho_f)(1 - \phi) = 0.01(1 - \phi)$ is very small and a large slip velocity is not required to levitate a particle. The calculation of the slip velocity ought to be defined in terms of time or ensemble averages at a fixed point, which are not readily calculated with the ALE method used here.

Figure 27 gives a scatter plot for the water flow in figure 18 ($\eta = 0.01$ poise, $R = 6 \times 10^4, G = 164$). The results here are what might be expected of turbulent flow and appear to represent the natural extrapolation of results given in this paper at lower Reynolds numbers. The relevant Reynolds number, based on the average particle velocity $\bar{U} = 200\,\mathrm{cm\,s^{-1}}$, the effective viscosity $\eta_m = 0.032$ poise and particle diameter d, is about 6000, a value at which we might expect weak turbulence. Informed readers will question the validity of our computation using Choi's (2000) split method in direct numerical simulation with no artificial viscosity or turbulence model. The natural way to test this result is to use mesh refinement. Our unstructured mesh is generated automatically from nodes on the surface of the circular particle. Our calculation converged, and converged solutions have nearly the same height history for 15–30 nodes on the circular particle when the timestep size (Δt) used is about 10^{-5} (the corresponding Courant number is about 0.1); the converged solution cannot be obtained when the number of nodes is less than 12 or sometimes greater

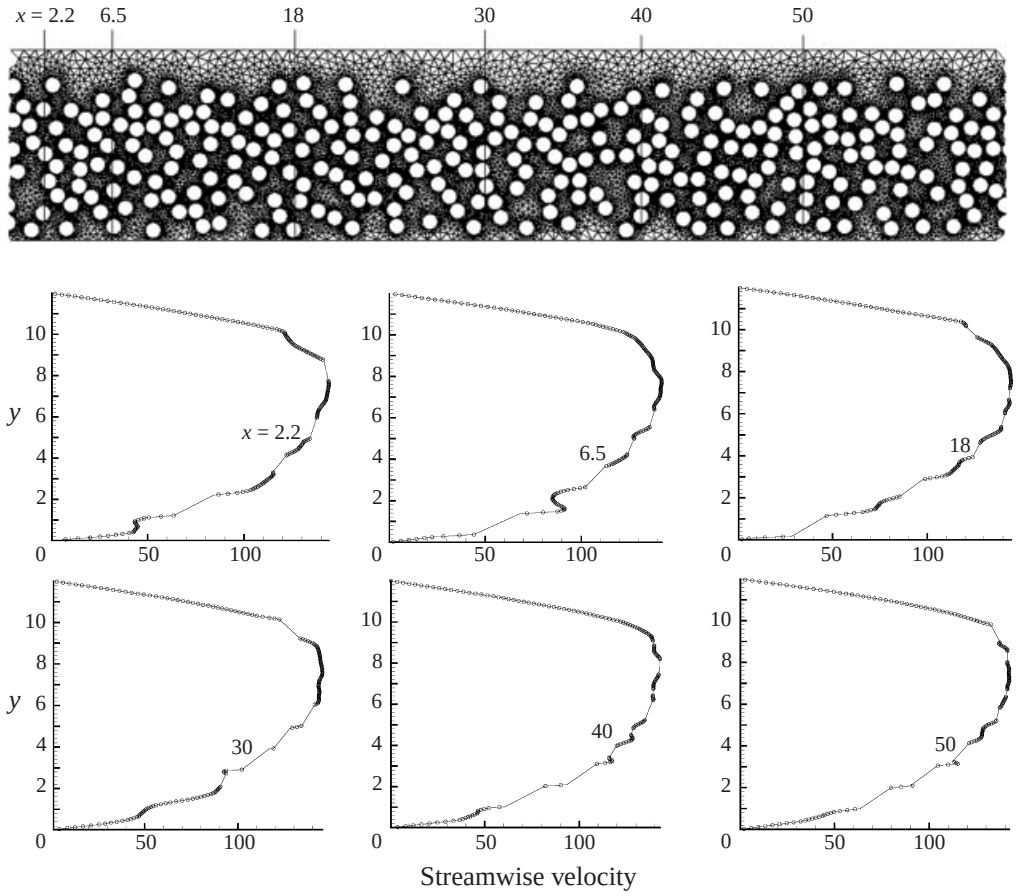

FIGURE 25. Fluid velocity profiles at 6 different sections of the flow of 300 particles at $\bar{p} = 20\,\mathrm{dyn\,cm^{-3}}$, $\eta = 1.0$ and when it is fully fluidized ($t = 28$).

than 30. When the number of nodes is greater than 30, the calculation may stop because the mesh generator is unable to generate mesh owing to the distortion of very short elements during motion. We have not established the validity of such a high Reynolds number computation, but the results do converge to something which appears reasonable and survives tests of mesh refinement.

5. Summary of results

1. A numerical package (Choi 2000) based on a splitting method, which is an extension of the numerical package developed by Hu, Joseph & Crochet (1992) for the direct numerical simulation of solid–fluid mixtures, is used to study the fluidization by lift of 300 particles.

2. The present problem is governed by a shear Reynolds number R and a gravity number G. The product $R_G = RG$ is a Reynolds number based on the sedimentation velocity of a sphere under gravity. This is a measure of the activity level and is small when the viscosity is large. The ratio R/G is a generalized Froude number. It compares the inertial lift due to the shear to the buoyant weight and is independent

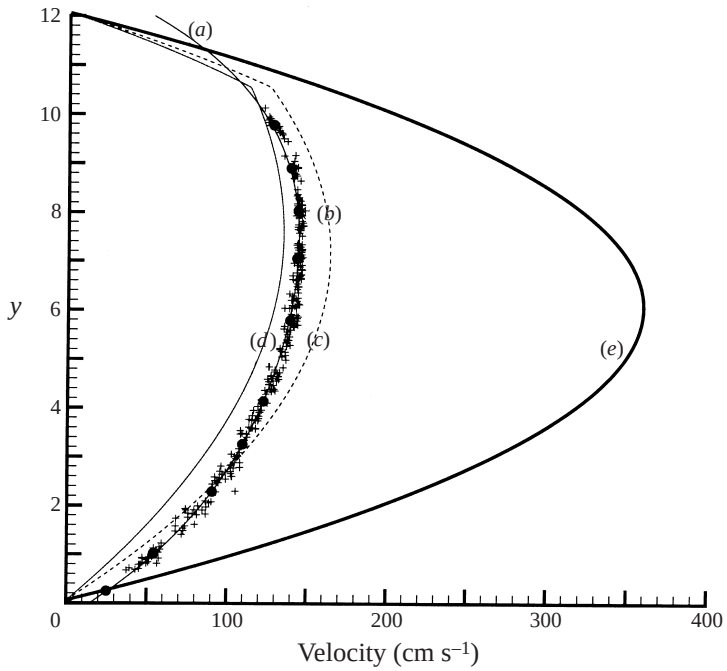

FIGURE 26. Scatter plot of +, particle velocities of 300 particles taken from figure 25 ($\eta = 1$ poise, $\bar{p} = 20\,\mathrm{dyn\,cm^{-3}}$); (*a*) ——, average particle velocity for the scatter; (*b*) average fluid velocity taken from the tecplots in figure 25 at 10 values of y over 1000 points; (*c*) two-fluid Poiseuille flow model based on (4.14) and (4.15) using the effective viscosity $\eta_m = 3.06$ from (4.12) with $\phi = 0.36$, and (*d*) $\eta_m = 4.19$ from (4.13); (*e*) undisturbed Poiseuille flow. The particles 'hold up' the fluid. The increased drag on the fluid owing to the free particles can be modelled as an effect of an increased viscosity of the fluid–solid mixture.

of viscosity; the rise of particles is large when this number is large even though the motion may be sluggish.

3. A turning point bifurcation of a steady forward flow of a single particle was found (see Patankar *et al.* 2001). The height and particle velocity change strongly at such points and the solutions may exhibit hysteresis. The proof that the arrangement of stable and unstable solutions is associated with double turning points is given by Patankar *et al.* (2001).

4. The transport of a slurry of 300 heavier-than-liquid particles in a plane pressure-driven flow was studied using DNS. Time histories of fluidization of the particles for three viscous fluids with viscosity $\eta = 1.0$, 0.2 and 0.01 (water) were computed at different pressure gradients. The time history of the rise of the mean height of particles at a given pressure gradient is monitored and the rise eventually levels off when the bed is fully inflated. The time taken for full inflation decrease as the pressure gradient (or shear Reynolds number) increases. The bed does not inflate when the critical value is below the critical value for lift off of a single particle.

5. At early times, particles are wedged out of the top layer by high pressure at the front and low pressure at the back of each particle in top row.

6. The dynamic pressure at early times balances the weight of the particles in the rows defining the initial cubic array. This vertical stratification evolves into a horizontally stratified propagating wave of pressure which tracks waves of volume fraction. The pressure wave is strongly involved in the lifting of particles. For low-

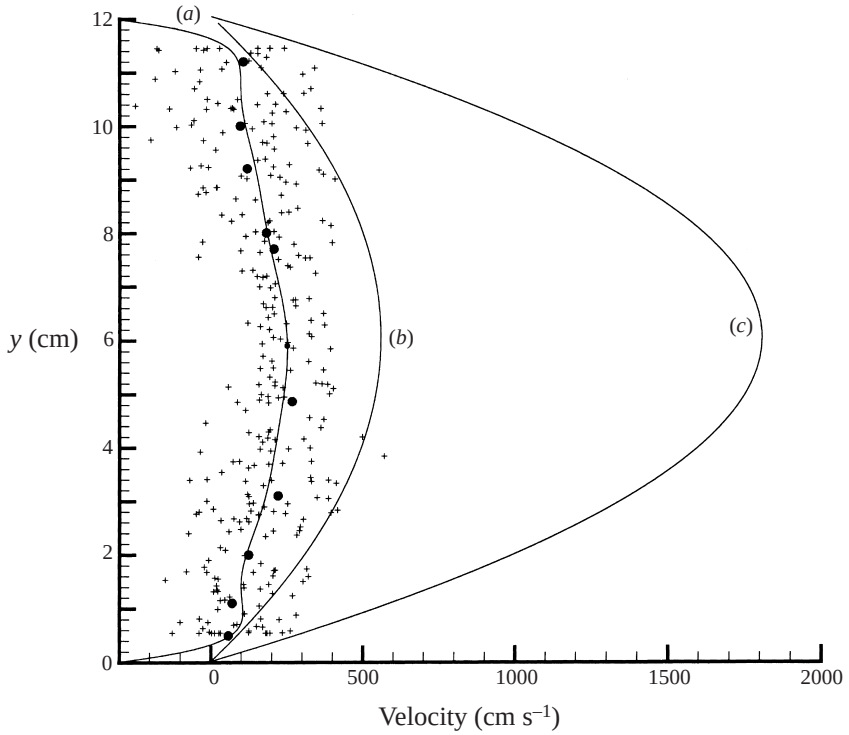

FIGURE 27. Scatter plot for the fluidization of 300 particles in water ($h = 0.01$ poise) shown in figure 18. In this case, particles fill the whole channel and the scatter is caused by large fluctuations. (*a*) The average velocity profile (——) is rather flat as would be expected from turbulent flow. •, average fluid velocities from the tecplots in figure 18. (*b*) Velocity profile for Poiseuille flow of a fluid with effective viscosity $\eta_m = 0.032$ given by (4.13) for $\phi = 0.31$. This does not agree with the simulation. Perhaps it would be better to create an effective 'eddy viscosity' theory for this weakly turbulent flow. (*c*) Undisturbed Poiseuille flow without particles.

viscosity fluids such as water where RG is large, the particle-laden region supports an 'interfacial' wave corresponding to the wave of pressure. If R/G is large, the interface collapses since the stronger lift forces push wave crests into the top of the channel, but the pressure wave persists.

7. A simple analytical model for the free motion of a single particle of diameter d in Poiseuille flow gives rise to a formula for the particle velocity

$$\frac{U_p}{U(y_1)} = \left(\frac{W+d}{W-d}\right)\left(\frac{y_1 - \frac{1}{2}d}{y_1}\right)\left(\frac{W - y_1 - \frac{1}{2}d}{W - y_1}\right),$$

where y_1 is the distance from the channel bottom to the particle centre, $U(y_1)$ is fluid velocity at y_1 when no particle is present and W is the channel height. The slip velocity $U(y_1) - U_p > 0$ is positive, but tends to zero with the particle diameter. The presence of particles produces a lag in the fluid velocity and the effect of such a drag can be interpreted as an effectively increased viscosity for the fluid–solid mixture.

8. DNS data can be sampled for average fluid and average solid velocities. The difference of these velocities is very small, but the difference between the composite velocity and the particle-free Poiseuille flow is dramatic. We attempted to model the average flow of the slurry by a two-fluid model in which the particle-laden region is

treated as a fluid with an effective viscosity; for this calculation we used two different well-regarded formulae for the effective viscosity with pure liquid above the mean height and effective liquid below. We would like to be able to predict the mean height from considerations involving an effective density.

This work was partially supported by the National Science Foundation KDI/New Computational Challenge grant (NSF/CTS-98-73236), by the US Army, Mathematics, the Engineering Research Program of the Office of Basic Energy Sciences at the DOE, by a grant from the Schlumberger foundation and from Stimlab Inc. and by the Minnesota Supercomputer Institute.

REFERENCES

Choi, H. G. 2000 Splitting method for the combined formulation of fluid-particle problem. *Comput. Meth. Appl. Mech Engng* **190**, 1367–1378.

Chorin, A. J. 1968 Numerical solution of the Navier–Stokes equations. *Math. Comput.* **22**, 745–762.

Hu, H. H., Joseph, D. D. & Crochet, M. J. 1992 Experiments and direct simulations of fluid particle motion. *Video J. Engng Res.* **2**, 17–24.

Joseph, D. D. 2000 Interrogations of direct numerical simulations of solid-liquid flow. http://www.aem.umn.edu/Solid_Liquid-Flows/references.html.

Kataoka, T., Kitano, T., Sasahara, M. & Nishijima, K. 1978 Viscosity of particle filled polymer melts. *Rheol. Acta.* **17**, 149.

Kern, L. R., Perkins, T. K. & Wyant, R. E. 1959 The mechanics of sand movement in fracturing. *Petrol. Trans. AIMechE* **216**, 403.

Patankar, N., Huang, Y., Ko, T. & Joseph, D. D. 2001 Lift-off of a single particle in Newtonian and viscoelastic fluids by direct numerical simulation. *J. Fluid Mech.* **438**, 67–100.

Richardson, J. F. & Zaki, W. N. 1954 Sedimentation and fluidization: Part I, *Trans. Instn Chem. Engrs* **32**, 35.

Thomas, D. G. 1965 Transport characteristics of suspension: VIII. A note on the viscosity of Newtonian suspension of uniform spherical particles. *J. Colloid Sci.* **20**, 267.

Wallis, G. B. 1969 *One-dimensional Two-phase Flow*. McGraw-Hill.